



HAL
open science

Strengthening of the hydrological cycle in the Lake Chad Basin under current climate change

Florence Sylvestre, Abdallah Mahamat-Nour, Toussaint Naradoum, Matias Alcoba, Laetitia Gal, Adrien Paris, Jean-François Cretaux, Binh Pham-Duc, Christophe Lescoulier, Romain Recouvreur, et al.

► **To cite this version:**

Florence Sylvestre, Abdallah Mahamat-Nour, Toussaint Naradoum, Matias Alcoba, Laetitia Gal, et al.. Strengthening of the hydrological cycle in the Lake Chad Basin under current climate change. Scientific Reports, 2024, 14, pp.24639. 10.1038/s41598-024-75707-4 . hal-04893535

HAL Id: hal-04893535

<https://hal.science/hal-04893535v1>

Submitted on 20 Jan 2025

HAL is a multi-disciplinary open access archive for the deposit and dissemination of scientific research documents, whether they are published or not. The documents may come from teaching and research institutions in France or abroad, or from public or private research centers.

L'archive ouverte pluridisciplinaire **HAL**, est destinée au dépôt et à la diffusion de documents scientifiques de niveau recherche, publiés ou non, émanant des établissements d'enseignement et de recherche français ou étrangers, des laboratoires publics ou privés.



OPEN Strengthening of the hydrological cycle in the Lake Chad Basin under current climate change

Florence Sylvestre^{1,2}✉, Abdallah Mahamat-Nour², Toussaint Naradoum³, Matias Alcoba⁴, Laetitia Gal^{5,6}, Adrien Paris^{5,6}, Jean-François Cretaux⁶, Binh Pham-Duc⁷, Christophe Lescoulier⁸, Romain Recouvreur⁸, Mahmoud Mahamat Ahmat³ & Djergo Gaya⁹

Central Sahel is affected by a reinforcement of rainfall since the beginning of 1990s. This increase in rainfall is affected by high inter-annual variability and is characterized by extreme rain events causing floods of unprecedented magnitude. However, few studies have been carried out on these extreme events. Moreover, with current climate change expected to strengthen the hydrological cycle, we don't know if these events could become more frequent. Here, we report the hydrological changes that currently occur in the Lake Chad basin. Based on ground observations and satellite data, we focused on the 2022 flood event, demonstrating that it was the most important event from the last 60 years, comparable to what occurred during the last wet period between the 1950s and the 1960s. We showed that under this precipitation regime and if warming is not regulated at a global scale, the return period of the 2022 major riverine flood is expected to be between 2 and 5 years. By using modelling experiments, our study also suggested that in the next decade, future flow rates of the main rivers draining the Lake Chad basin could reach the values observed in the 1950s. These results strongly suggest anticipating water management in a context of poor infrastructural development.

Central Sahel is affected by a multidecadal wet and dry alternating period¹. During the twentieth century, this region experienced at least two wet phases, the last and most important of which occurred from the 1950s to the 1960s². This wet period was followed from the 1970s to the 1990s by severe and dramatic droughts³, which are recognized as the largest climatic signals ever recorded over such large areas since the observation period^{4,5}. However, after the 1990s, partial rainfall recovery occurred, resulting in the greening of Sahel⁶. Although this trend is affected by high interannual variability, it has been confirmed since the mid-2010s⁷. This period is particularly characterized by extreme rain events⁸. It is estimated that these extreme events represent 90% of the rain causing floods of unprecedented magnitude⁹. For example, the city of Ouagadougou in Burkina Faso experienced heavy flooding in 2009 following a 10-h rain event that totalled 263 mm. This event resulted in the displacement of 150,000 inhabitants and destroyed many infrastructures¹⁰. Similarly, in 2010 and 2012, Niamey in Niger experienced the largest floods ever recorded since the observations began in 1929¹⁰. These events are generally reported in the media and in reports from humanitarian nongovernmental organizations. However, few scientific studies have been conducted on flood characterization and its consequences for the population (loss of life, destruction of houses and infrastructure) and on the rainfed agriculture that characterizes this region¹¹. In addition, with recent climate modelling experiments predicting an increase in precipitation by +30% by 2050¹², documenting what is currently happening in the central Sahel and what could be expected in the context of ongoing global warming is crucial.

In 2022, Sahel from Senegal to Chad was particularly affected by both fluvial and pluvial (rainfall-related) flood events¹³. This year was characterized by an earlier rainy season onset and an amount of precipitation above normal in many regions. This situation was anticipated by the Regional Climate Outlook Forum for West Africa, which issued an alert in early May on the risk of a longer and more intense rainy season than normal¹⁴. With at least 612 and 195 fatalities, respectively, the floods over Nigeria and Niger are among the deadliest in the country's history^{15–17}. The devastation in Nigeria is worse than that in the 2012 flood disaster¹⁸, in which

¹Aix-Marseille Université, CNRS, IRD, INRAE, CEREGE, Aix en Provence, France. ²Laboratoire Hydro-Géosciences et Réservoirs, Université de N'Djamena, N'Djamena, Tchad. ³Ministère de l'Eau et de l'Energie, Direction des Ressources en Eaux, N'Djamena, Tchad. ⁴Toulouse, France. ⁵HydroMatters, Le Faget, France. ⁶Laboratoire d'Etudes en Géophysique et Océanographie Spatiales (LEGOS), Université de Toulouse, CNES/CNRS/IRD/UT3, Toulouse, France. ⁷REMOSAT, University of Science and Technology of Hanoi, Vietnam Academy of Science and Technology, Hanoi, Vietnam. ⁸EGISWater and Maritime, Montpellier, France. ⁹Agence Nationale de la Météorologie, N'Djamena, Tchad. ✉email: sylvestre@cerege.fr; florence.sylvestre@ird.fr

34 out of 36 states and more than 3.2 million people were affected—including 1.5 million displaced and 2.776 injured^{19,20}. Several hundred thousand hectares of land have been inundated, causing damage to more than 300 thousand homes and more than half a million hectares of farmland.

The Lake Chad basin is one of the areas that was strongly impacted by this event. Occupying an area of 2,500,000 km², it is now hydrologically active only in its southern area, which is characterized by a Sudanese climate and drains the rainfall received over an area of 610,000 km². In 2022, 19 out of 23 provinces located in the southern part of the basin were flooded, with more than 1,468,847 people affected and 350,000 ha of land devastated²¹. Due to its location at the confluence of the Chari and Logone Rivers, the capital, N'Djamena, is an extremely exposed city. In 2022, 254,483 people were affected and supported by the humanitarian system²¹. On October 2023, 19th, Chad declared a state of emergency²².

In this report, we focused on fluvial floods. We used ground observations based on gauge stations from the hydrological network of the Chari and Logone Rivers complemented with satellite observations, especially for Lake Chad, which is still poorly monitored (see “Methods”). Using optical imagery from the Moderate Resolution Spectroradiometer (MODIS) and time series of lake water levels derived from multitemporal altimetry satellites (i.e., TOPEX/Poseidon, ENVISAT, Jason-2 and -3, SARAL, Sentinel-3A, and Sentinel-6A), we reconstructed the surface water extent and level of the lake until December 2022. These methods have already been tested in a previous study demonstrating their validity for estimating open water surfaces compared to surfaces covered by vegetation²³; lake Chad, which is in a flat landscape, is a shallow lake partly covered by aquatic vegetation that could partly hamper good estimations of the water surface by satellite survey.

The Lake Chad Basin: a hydrological giant in central Sahel

The Lake Chad drainage basin covers 2.5 million km², representing 8% of the African continent (Fig. 1). It is a hydrologically closed drainage system located at the southern fringe of the Sahara in the Central Sahel region of northern Africa. The basin features a Sudanese climate in the southern region and a semiarid climate in the northern region. The climate is tropical with two seasons. The wet season begins in May and ends in October, and most of the precipitation falls in July and August. Evaporation rates show a strong seasonal cycle that follows changes in the air temperature²⁴.

Today, water intakes come from the southern portion of the drainage basin and are transported by river discharge from the Chari-Logone system, the Komadougou Yobe River located in Niger and by precipitation on the lake surface (Fig. 1). Even if the Chari-Logone River system covers only 25% of the lake Chad basin, it accounts for up to 82% of the lake water supply²⁵. The Chari and Logone Rivers drain a watershed with an area of 610,000 km² located between 5° N and 12° N (Fig. 1). The Logone River, with a length of 1000 km, originates on the Adamawa Plateau in Cameroon and has an altitude ranging from 305 to 835 m²⁶. The total area of the Logone catchment is 90,000 km². The Chari River starts in the Central African Republic at an altitude ranging from 500 to 600 m, and it flows nearly 1200 km. The Chari Basin covers an area of approximately 523,000 km². Both rivers converge at N'Djamena before reaching Lake Chad, 110 km downstream of the city (Fig. 1). Based on river discharge time series, eight subbasins were delineated, and their contributions to the debit flow were estimated²⁴.

Lake Chad is the terminal lake of this drainage basin system. Today, it is a shallow lake (<3 m) subdivided into two main areas most of the time, the northern and southern pools, which are separated by an east-west vegetation-covered sand barrier known as the Great Barrier. The northern pool has an altitude of 275.3 m, whereas the southern pool is located at 278.2 m and the great barrier is located at 279.3 m²⁶. The inputs from

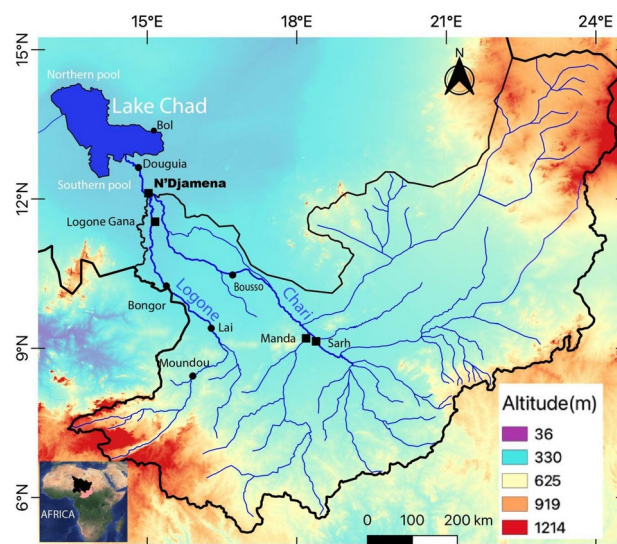


Fig. 1. Location of the Chari-Logone basin in central Africa, south of the Lake Chad Basin, corresponding to the present hydrologically active basin (SRTM Topo 30 <https://earthexplorer.usgs.gov/>, QGIS 3.4.5). The main gauge stations are indicated by squares. The main cities are indicated by circles.

the rivers in the lake are balanced by evaporation, estimated at more than 2000 mm/year, and by seepage to groundwater²⁷.

The lake Chad basin is considered as a good sensor of climate^{25,27}. Studies have investigated the role of anthropic activities on the runoff and flow of the main tributaries, demonstrating that there is no clear evidence of an anthropogenic impacts, e.g. withdrawal for domestic and cropping uses, responsible for a decrease in flows or a modification of the hydrological regime in the Chari-Logone basin²⁴. Moreover, the basin has been poorly managed, any hydraulic infrastructures have been built and the few managements existing do not imply a modification of the river flow.

2022: The greatest flood recorded in the Lake Chad basin since the 1960s

The flood hydrograms from the Chari and the Logone are derived from data recorded by gauge stations located in the Lake Chad Basin (Fig. 1). These gauge stations are read daily at the same time at 8 a.m. GMT +0. The level of the rivers was measured in meters above the zero reference point when the limnometric scale was used (see “Methods”). Here, we focused on the gauge station from N’Djamena (named N’Djamena TP), which is located 2.4 km downstream of the confluence of the Chari and the Logone at 288.58 m. We also used the gauge stations located at Sarh and Manda located upstream in the southern part of the basin at 355.18 m and 354.11 m, respectively (Fig. 1). Both stations represent 58% of the flow rate from the Chari River²⁴. From Logone, we used the Logone Gana station, which is located at 295.21 m and reflects 34% of the water input for this river.

The 2022 hydrological season in the southern basin began in early June (Supplementary Fig. S1). At Sahr, the level of the Chari increased slowly until the end of May, starting at 1.50 m before accelerating after this month. It quickly reached 2.32 m on July 23, 2021, and then increased steeply until October 16, 2021, when it reached its maximum at 7.14 m. Then, it decreased until the end of the dry season at the end of April 2023. In Manda, we observe the same dynamics, with an acceleration of the river flow occurring slightly earlier between July 10 and 12, 2022 (Supplementary Fig. S1). We also observe a period of high variability between August 9 and 28, 2022, at the Manda gauge station. Then, the level increased steeply, reaching its highest level on October 4, 2022, at 7.27 m, slightly earlier than in Sarh.

From the Logone River at Logone Gana station (Supplementary Fig. S1), the level began to rise slowly at the end of May and then rose very quickly until the end of August, when it reached an average of 2 cm per day. The increase in river level then slowed to less than 1 cm per day. The peak flood occurred between October 23 and November 12, 2022, oscillating between 6.19 m and 6.23 m.

At N’Djamena, as in the southern part of the basin, the river level started increasing slowly in June (Fig. 2). A first increase in the level was recorded early in August; it slowed at the beginning of September before a rapid increase until October 22, 2022. At this elevation, it lasted until October 30, 2022. Then, it decreased at 8.02 m on November 6, 2022, before continuing to increase until it reached its highest level on November 13, 2022 at 8.14 m. After this date, the level decreased rapidly.

In N’Djamena, we have a record of the river level since 1933 (Supplementary Fig. S2), suggesting a historical perspective. When comparing the level reached in 2022 with that in this time series, we observed that the year 2022 was the year with the greatest difference recorded over the last 60 years. In 1961, the elevation of the Chari River reached 9.10 m, the wettest year recorded during the last ninety years (Fig. 2). This corresponded to a flow rate recorded at 5160 m³/s (Supplementary Fig. S3). The years when the Chari level exceeded 7.50 m at N’Djamena were considered to be very wet years because significant impacts were observed. During recent decades, the two wetter years recorded before 2022 were 2012 and 2020, with heights of 7.66 m and 7.47 m, respectively (Fig. 2). The flow rates recorded in 2012 and 2020 were 3548 m³/s and 3409 m³/s, respectively. The years 1988 and 1998, with 7.58 m (3472 m³/s) and 7.33 m (3311 m³/s), respectively, were also characterized by a strong rainy season, especially 1988, which occurred during the dry phase (Supplementary Fig. S2). However, for that year, we have no records about the societal impacts.

Lake Chad, the outlet of the Chari-Logone rivers, expands according to water inputs. In 2022, the water level of the lake started to increase beginning in the middle of August, reaching its maximum at 3.3 m recorded at the Bol gauge station on December 16, 2022 (Supplementary Fig. S4). After this date, it decreased slowly until April 2023. The delay observed between the maximum level of Chari at N’Djamena (Fig. 2) and the maximum level of Lake Chad was approximately one month (Supplementary Fig. S4). This delay usually corresponds to the timing of water transfer from Chari to the lake^{7,25,26}. We completed these ground observations with MODIS imagery to estimate its maximum extent, including the southern and northern pools. In 2022, the maximum surface water extent, without vegetation, was 5370 km² (Fig. 3). This corresponds to a 24.76% increase compared to the average annual maximum lake extension for the 2012–2022 period, which was approximately 4310 km² (Pham et al., 2020). However, for obtaining a total estimation of the water extent of the lake, it is necessary to consider the water covered by vegetation. Then, the total surface water area reached 18,800 km², corresponding to an extension of approximately 7.5% compared to the mean annual maximum of the lake during the 2012–2022 period, which was approximately 17,500 km². During the wet 1950–1960 observation decades, it was estimated that the lake area reached 25,000 km². Using satellite altimetry data (see “Methods”), the lake reached a maximum level of 281.36 m in December 2022. In 1963, the maximum level was 282.48 m, and in 1973, it was 281.47 m²⁶.

The impact of global climatic change

Precipitation in tropical Africa results from a combination of factors, including the monsoonal on-land flow of moist air, low-level convergence of air at the intertropical convergence zone and, of particular importance, the deep vertical motion of air, which is modulated by the interaction of the Tropical Easterly Jet (TEJ) and the African Easterly Jet (AEJ) over northern Africa²⁸. The monsoon circulation is driven by the thermodynamic contrast between the cooler ocean (the equatorial Atlantic) and an intense heat low (the Saharan heat low),

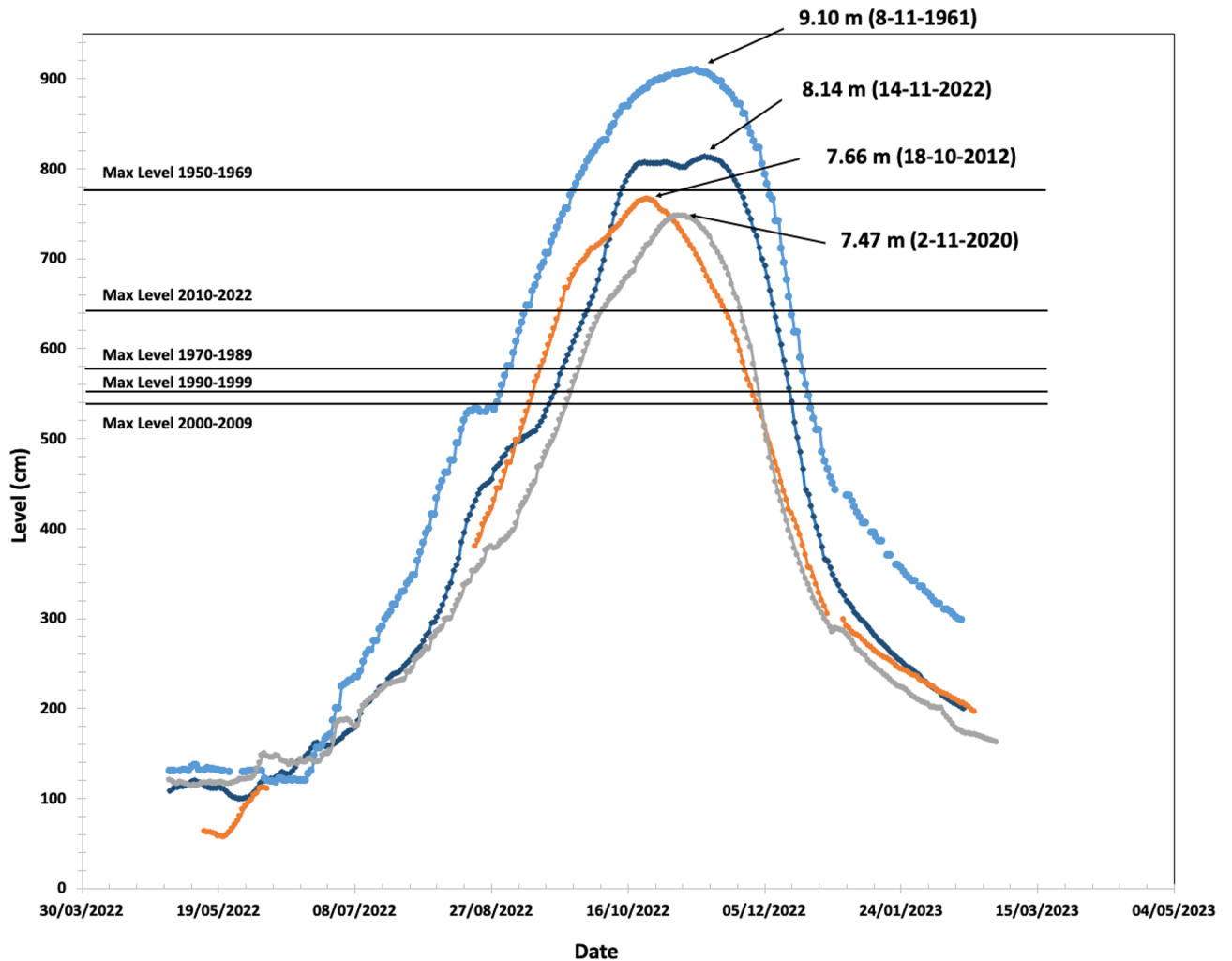


Fig. 2. Hydrogram of N'Djamena (gauge Station N'Djamena TP) for 2022 compared with 1961, 2012 and 2020. The plain lines indicate the mean maximum level measured during the decades 1950–1969, 1970–1989, 1990–1999, 2000–2009 and 2010–2022.

which develops over the western Sahara during the boreal summer. Southwesterly winds are established between the equatorial Atlantic and the Saharan heat low, bringing moisture to the continent²⁸. The African Easterly Jet (AEJ) is also driven by the low-temperature gradient from the Gulf of Guinea to the Sahara Desert. Associated with easterly waves, these synoptic-scale disturbances propagating westwards on the AEJ, from central and eastern Africa across West Africa and into the tropical Atlantic, are characterized by a peak in convection and precipitation²⁹. Moreover, since the beginning of the century, Central Sahel has experienced a new era of climate extremes characterized by a transient state combining a rarefaction of rainfall occurrence and a reinforcement of rainfall intensities³⁰. The average intensity of rainy events has increased, especially for the largest rainy events at daily and subdaily timescales³¹. The 2022 rainy season was characterized by mixed conditions. Flooding occurred because of above-average rainfall reinforced by extreme events. These events are attributed to mesoscale convective systems (MCSs), which tend to increase their vertical development, favouring convergent humidity and producing exceptional cumulative rainfall⁹. A warmer Sahara intensifies convection within Sahelian storms through increased wind shear and changes to the Saharan air layer, leading to more intense, heavy precipitation.

For 2022, climate change is estimated to emphasize the rainfall event by approximately 80 times, leading to an increase in intensity of approximately 20%³². The seasonal rainfall increases significantly due to rising global temperatures, as confirmed by observations over the Lake Chad catchment³². The return time of the 2022 event was estimated to be approximately 1 event in 10 years, with rainfall increases ranging between 30 and 40%. Moreover, the most recent experiments further noted that tropical sea surface temperatures and associated dynamic changes could increase rainfall in central Africa, even if rainfall projections are uncertain because of contrasting signals from models with especially large discrepancies during the main rainy season³³. From ground observations, the mean annual observed rainfall in N'Djamena has increased since 2018 (except for 2021), whereas in Sarh, which is south of Chad, this trend is pronounced (Supplementary Fig. S5).

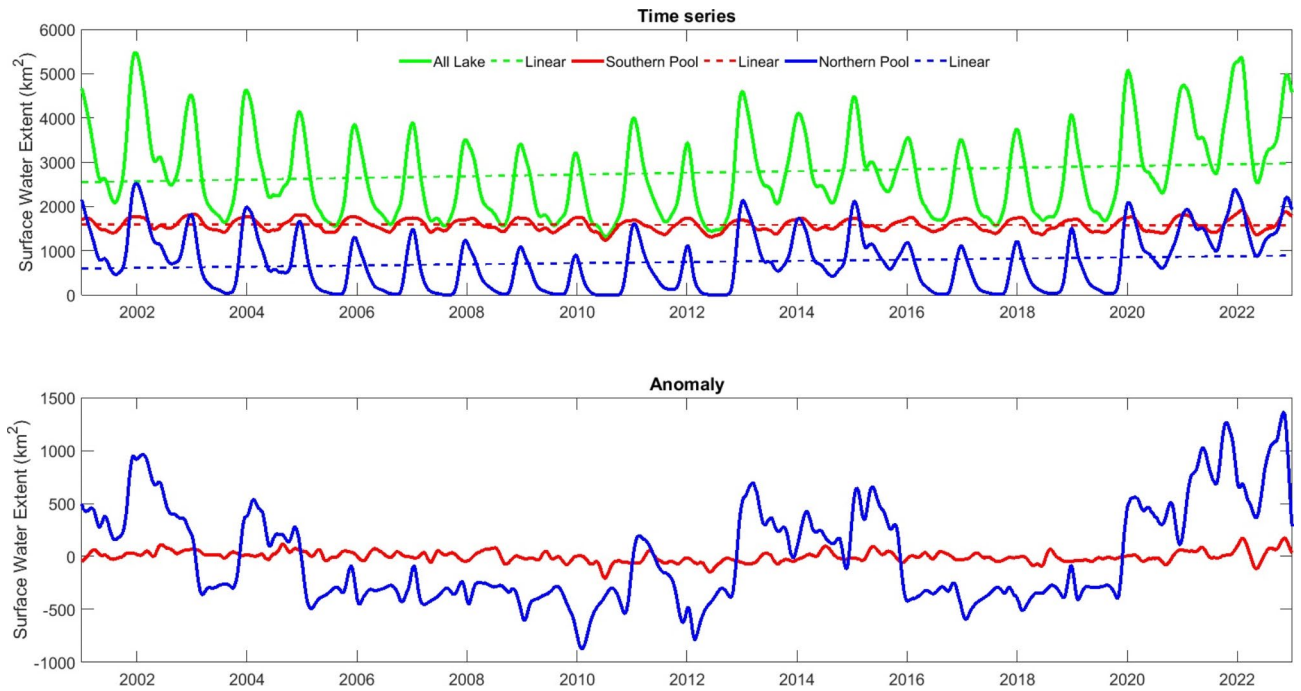


Fig. 3. Time series (top) and anomalies (bottom) of the surface water extent in the northern pool (blue), southern pool (red) and Lake Chad (green) for the 2001–2022 period. The linear trends are also plotted.

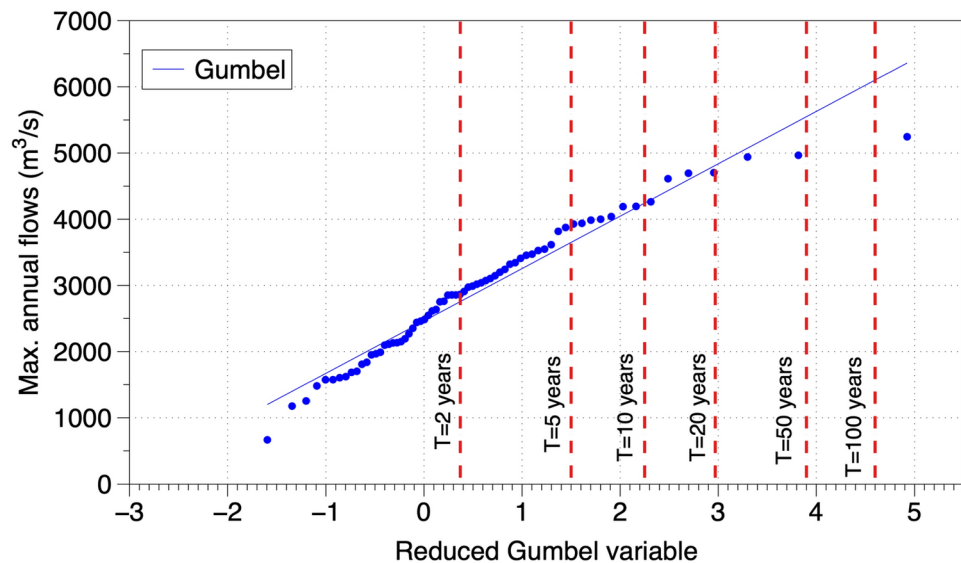


Fig. 4. Return period for historical floods based on the distribution function of Gumbel.

The challenges of water management

In this context, it is crucial to obtain the best estimation of these recurrent flooding events for the next few decades. We first estimate the historical flood return period based on the maximum flow rates observed at N'Djamena between 1960 and 2022 (see “Methods”). We estimated that the historical floods of 2012 (3548 m³/s measured in November), 2020 (3409 m³/s measured in November) and 2022 (3986 m³/s measured in November) had return periods between 2 and 10 years (Fig. 4). A statistical analysis of the flow data revealed that for a return period of 2 years, the maximum observed flow reached 2753 m³, which was comparable to the values recorded in 1958 (2802 m³/s), 1968 (2781 m³/s) and more recently in 2018 (2760 m³/s). For a 20-year return period, the maximum flood is 4814 m³, comparable to the flow rate observed during the moister decades in 1950 (4400 m³/s) and 1960 (4008 m³/s). In 1961, the maximum recorded flow rate was 5156 m³/s (Supplementary Fig. S3; Supplementary Table S1).

We completed these estimations by predicting the future flow rate of the Chari–Logone River system. A hydrological model developed at the scale of the Chari–Logone basin using the ‘Modèle Grand Bassin’ (MGB) was first developed (see “Methods”). Qualitative analysis based on four performance criteria highlights the confidence in the accurate representation of hydrological processes across the whole basin (Supplementary Table S2). For the N’Djamena station, the model adequately represented the general dynamics of discharge with good representations of low and high flows (Supplementary Fig. S6). The uncertainties in the simulations are estimated to be approximately 17% and 12% compared to the observed values when the 5th and 95th percentiles are considered for the observations and simulations, respectively. Then, we selected five CMIP6 models and two shared socioeconomic pathway scenarios (e.g., the SSP2-4-5 medium forcing scenario and the SSP3-7-0 high forcing scenario) to predict the Chari–Logone flow rates for the prospective 2040–2060 decade (Supplementary Table S3; see “Methods”). Figure 5 shows that historical data tend to underestimate low flow rates, especially moderate flow rates ($< 3000 \text{ m}^3/\text{s}$), and conversely overestimate high flow rates ($> 3000 \text{ m}^3/\text{s}$). However, compared to the observations, the climate projections from the ‘ipsl,’ ‘mirc,’ and ‘nesm’ models consistently yield significantly greater flow rates across all flow rate ranges. Regarding the results from the ‘access’ model, we observe that the estimations align more closely with the current observations. Additionally, there is a noticeable decrease in flow rate compared to that of the observations in the case of the ‘cmcc’ model. Figure 6 shows the results of the corrected flow quantiles Q_F^c for the 10- and 5-year return periods. Note the crossover of the curves for the recent period by construction. Models struggle to reproduce the wet/dry cycle observed in the 1950s and 1990s. However, despite these uncertainties, the simulation outputs under the constraints of climate change from two selected scenarios revealed a clear increase in average flow rates over the prospective period of 2040–2060, particularly a significant increase in peak flow values, surpassing the annual mean value almost every year for most models. For the 2050 horizon, the return flows are approximately the same as the level of return flows observed in the 1950s, the most recently observed wettest period. It is worth noting that the climatic signal of wetter central Sahel in the future from CMIP6 models is characterised as ‘low confidence’ by the IPCC report due to the variability between CMIP6 models and between regional (CORDEX) and global experiments (CMIP6) (6th report section 12.4.1.2). From IPCC 6th report, increasing precipitation for a 1.5 °C and 2 °C global warming levels are found in central and eastern Sahel with low confidence and the wet signal is getting stronger and more extended for a 3 °C and 4 °C warmer world. Although rainfall is not a robust variable in climate projections, we believe that the impacts of such an increase should be taken into account.

As observed, the limitations in accurately representing certain years in the current climate may be attributed to the choice of precipitation input data for the model. The use of long-term data is often associated with reduced interannual variability. Therefore, it would be worthwhile to work with improved rainfall datasets at finer spatial and/or temporal scales to better capture the interannual variability in climate events and, consequently, hydrological phenomena. Regarding the current period, it would be practical to verify whether the rating curves used to estimate flow rates require recalibration, especially for a better understanding of low-flow conditions. Concerning the negligible impact of the new land use map for 2050 on flow predictions (Supplementary Fig. S7), it would be interesting to conduct a similar analysis while increasing anthropogenic areas near water bodies to assess sensitivity, regardless of the precipitation dataset used.

To ensure that projection models align with observational reality for past periods and are capable of forecasting future river floods in N’Djamena, it would be useful to implement dichotomous prediction methods using a threshold, for instance, probability of detection (POD) indices or false alarm rate (FAR) indices. Preliminary tests were conducted using these two methods to compare observed data and historical data from various

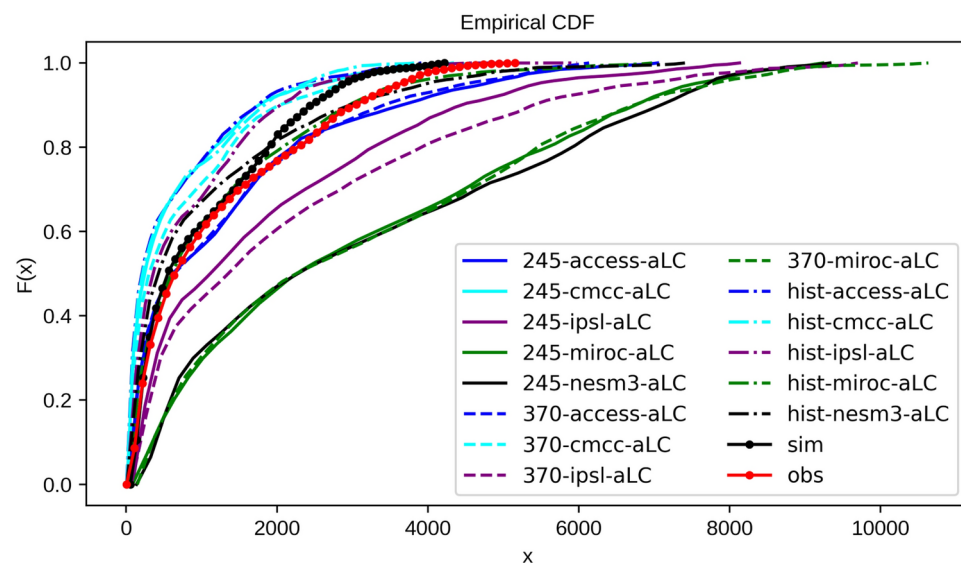


Fig. 5. Outputs from projection models (2040–2060), historical CMIP6 data and observations (1950–2014) at N’Djamena based on MGB simulation.

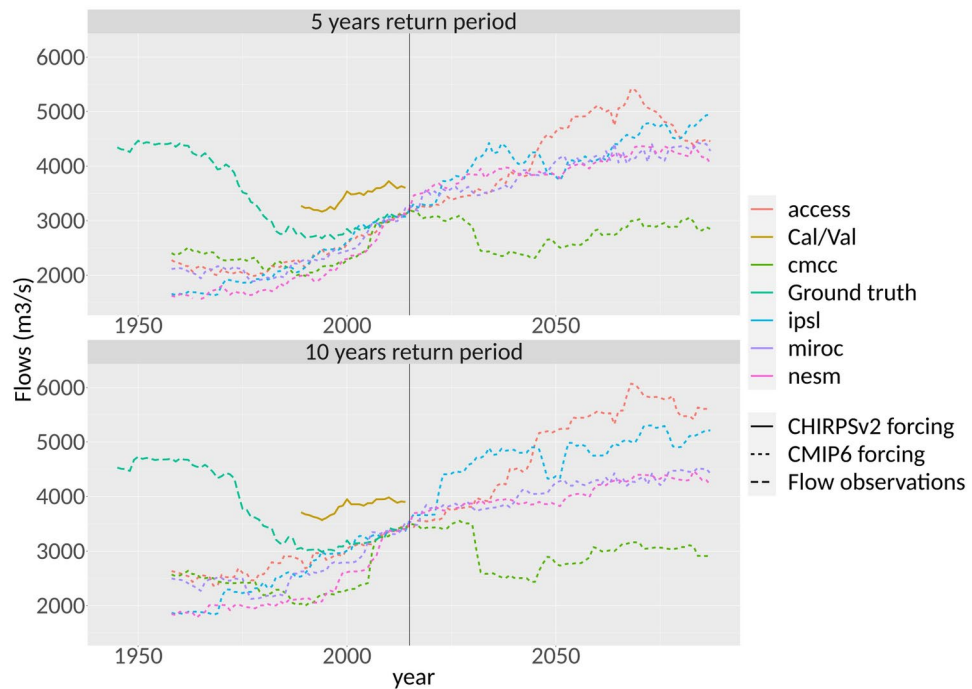


Fig. 6. Evolution of peak flows at 10- and 20-year return periods between 1933 and 2100. The pink curve shows the evolution of the Q_0 observations. The brown curve shows the Q_R reconstructed flows (model + observations). The colour curves show the flow rates from the forced MGB with CMIP6 models. Before 2015, these are the historical Q_H flows, and after 2015, the prospective Q_F flows are for the SSP245 scenario.

CMIP6 models for the period of 1950–2013, with a defined threshold of 3000 m^3/s (Supplementary Table S4). False alarms are prevalent across all the models, indicating a trend towards overestimating flood peaks, even in the past, and detecting an excessive number of flood events compared to reality.

Despite the uncertainties in climate modelling experiments, our results show that the trend of increasing flood events has been confirmed in response to the intensification of the hydrological cycle in the context of ongoing global warming. For the Lake Chad basin, we observed the important and dramatic consequences that these events had on the Sahelian economy and on populations. The Chari and Logone Rivers are poorly regulated, which makes the Lake Chad Basin highly vulnerable. The southern part of Chad, which is the most populated area of the country and the most productive in terms of livelihoods, is strongly impacted. Additionally, the city of N'Djamena located on the shore of Chari after the confluence with the Logone was truly exposed. Historically, the city first developed in the downtown centre in the western part of the current city. However, during the dry decades of the 1970s and 1980s, the city was urbanized in the flood-prone areas of the Chari and Logone confluence, making neighbourhoods extremely vulnerable. These areas are currently home to approximately 300,000 inhabitants and are among the poorest³⁴.

Due to inevitable climate change and variability, long-term policies appear to be the only way to reduce the exposure of infrastructure and people to flood-prone areas. Based on our study and the models we developed, we recommend stepping up the monitoring of the basin. Our models can be used to improve river flood forecasting and to build early warning systems, helping for preventing floods for instance at N'Djamena city. We know that it takes three weeks for water to be transferred from the south of the basin, e.g. Sarh, to N'Djamena²⁴. By applying the MGB model, this forecast could be reinforced. Moreover, combining with the spatialisation of land use, this could provide an interesting tool for considering the siting of hydraulic infrastructures in view of the water management. This could help for considering their best location and sizing according to the areas that could be flooded regularly and the areas that could be preserved for instance for cropping.

Otherwise, from a more global perspective, unlike central Sahel, it is expected that the continent's Mediterranean margin could be affected by severe droughts in the next 30 years³⁵. The estimate of water stress for 2040 shows that central Sahel will become a region with excess water. Thus, water management in this basin is challenging because it could become an attractive area for climate migrants.

Methods

Gauge station network and collection of data

The network of hydrological stations included 20 hydrological stations located on the rivers of the Lake Chad basin (the Chari and Logone Rivers) (Fig. 1 main text). Most of them correspond to the limnometric scale read by an observer. These gauge stations measure the water height of the river. During the year, the hydrological

data are transmitted by monthly mail to the 'Direction des Ressources en Eau (DRE)' located at N'Djamena. However, during the rainy season, the transmission of data is performed daily by phone call with each observer.

Since the beginning of hydrological observations in 1950, the data have been stored in a database developed by the Institut de Recherches pour le Développement (IRD), named HYDROMET. This database also stores data from the early twentieth century (1933–1950), corresponding to the first observations obtained by the first scientific missions²⁶.

Satellite observations and satellite altimetry data

Moderate resolution imaging spectroradiometer (MODIS) land-surface reflectance satellite observations

MODIS is an important instrument of NASA's Terra satellite (launched on 18 December 1999) and NASA's Aqua satellite (launched on 4 May 2002) and is used for earth and climate measurements. Both satellites follow a sun-synchronous, near-polar orbit at an altitude of approximately 705 km. Their design ensures that the Terra satellite passes over the equator from north to south at 10.30 a.m. (local time), while the Aqua satellite traverses from south to north at 1.30 p.m. (local time). With their combined capabilities, these two satellites can completely cover the entire surface of the Earth every 1–2 days. In this study, the authors utilized the MODIS/Terra (MOD09A1) atmospherically corrected land surface reflectance 8-Day Level 3 Global 500 m products version V061 to map and monitor monthly variations in the surface water extent of Lake Chad from 2001 to 2022. Each MOD09A1 image was carefully selected from the best Level-2 gridded (L2G) observation within an eight-day period, considering factors, such as high observation coverage, low view angle, absence of clouds or cloud shadows, and aerosol loading³⁶. The MODIS observations utilized in this study were obtained at no cost from NASA's Earth Data Hub (<https://search.earthdata.nasa.gov/search>).

Water level of Lake Chad derived from hydroweb

A time series of Lake Chad's water height, provided by the Hydroweb project (<https://hydroweb.next.theia-land.fr/>) was utilized to regularly monitor the variations in the lake's water level. This time series was derived from multialtimetry satellites (i.e., TOPEX/Poseidon, ENVISAT, Jason-2 and -3, SARAL, Sentinel-3A, and Sentinel-6A) and was processed, validated and distributed by the Hydroweb portal, which is part of the THEIA pole of earth observations.

Mapping the variation in the surface water extent and volume of Lake Chad

The methodology utilized to monitor the variations in the extent and volume of surface water in Lake Chad was described in previous publications^{23,37}. Here, we briefly present the method, which includes three main steps. First, using MODIS observations, we classified the surface around Lake Chad into one of four classes: open water (100% of the area is inundated), mixed water/dry land/aquatic vegetation (18% of the area is inundated²³, vegetation, and dry land). The blue band (band 3) was utilized to identify potential cloud pixels (where its surface reflectance values ≥ 0.2)³⁸; then, these corresponding values in all bands were removed and filled using the simple weight smoothing function before being used for the classification step. The criteria utilized for classification are presented in Supplementary Table S4, where Band 5 is the near-infrared (NIR) band, and the NDVI was calculated as the ratio between the red band (band 1) and the NIR band. Second, a time series of Lake Chad's water level, provided by Hydroweb (<https://hydroweb.theia-land.fr/>), was postprocessed to remove outliers and fill in missing values (if any). Third, time series of water extent and water level during the 2002–2022 period were converted to monthly time scales, and then, they were used as inputs to estimate the monthly variations in Lake Chad's water volume using Eq. (1)³⁹:

$$\delta V(i, i-1) = \frac{(H_i - H_{i-1}) \times (S_i + S_{i-1} + \sqrt{S_i \times S_{i-1}})}{3} \quad (1)$$

where δV is the lake's volume variation between two consecutive months ($i-1$ and i) and S and H are the corresponding surface water area and water height, respectively, of Lake Chad for months $i-1$ and i .

Determination of the flood return period

Extreme value distributions play a central role in hydrology, particularly in flood estimation. Gumbel's law is used to study the distribution of extreme values. Gumbel's law is the first extreme value law to be used to study annual maxima. Since the annual maximum of a variable is the maximum of 365 daily values, this law must be able to describe a series of annual maxima. It is a two-parameter law, with a position parameter (a) and a scale parameter (b).

The distribution function of the Gumbel distribution is expressed as follows (Eq. 2):

$$F(x) = \exp\left(-\exp\left(\frac{-x-a}{b}\right)\right) \quad (2)$$

a is the position parameter and b is the scale parameter, assuming the reduced variable (u) according to Eq. (3):

$$u = \frac{x-a}{b} \quad (3)$$

Then, the distribution is written as $u = -\ln(-\ln(F(x)))$. The advantage of using the reduced variable is that the expression of a quantile is linear.

Chari-Logone discharge modelling and prediction

The MGB model

The MGB model is a physically based large-scale distributed hydrological model developed by IPH^{40–42} in Porto Alegre, Brazil. It was initially designed for use in major Brazilian river basins and to overcome the limitations of sparse in situ data availability⁴¹. The input data for the MGB are divided into two categories: dynamic data, such as climate variables (precipitation, temperature, wind speed, relative humidity, atmospheric pressure, and sunshine duration) or vegetation variables (LAI, albedo, surface resistance, and vegetation height) and static data, such as soil type, land use, and elevation models.

This model consists of four modules designed for the calculation of the soil water balance, evapotranspiration, the propagation of fluxes within grid cells, and the routing of fluxes through the drainage network. The basin is divided into hydrologically similar surface elements or hydrological response units (HRUs)⁴³ that are used for hydrological classification and water balance computation. Each of these elements, commonly referred to as "Minis," is characterized by a unique combination of soils and land cover (classified into one or more classes) and is interconnected by channels with an average length of 10 km.

The main soil types in the Chad Basin were grouped into two classes based on their runoff generation potential. These classes include soils with low infiltration capacity (LIC) and soils with high infiltration capacity (HIC). The land use and land cover types were classified into five classes as follows: forest (F), shrubland (S), grassland (G), cropland (C), bare soil (B), wetland (W1), and water (W) (Supplementary Fig. S6). In addition to cartographic data, the model uses gridded daily precipitation and monthly data for temperature, solar radiation, relative humidity, wind speed, and atmospheric pressure. The atmospheric data were obtained from the ERA5 database for the calibrated version, CHIRPSv2 for the precipitation data and the CMIP6 database for climate projection models (databases available on Copernicus <https://cds.climate.copernicus.eu/>). CHIRPSv2 is based on infrared observations (e.g., Meteosat) corrected with surface rain gauges; thus, it is available for the whole Meteosat period (from 1981).

Calibration–validation of the MGB model

To assess the model's ability to simulate the hydrological system's dynamics at the outlets of the Chari and Logone Rivers, model calibration was performed for a specific period and validated for another period over 13 stations. The validation step confirmed the accuracy of the calibrated model parameters for simulating stationary processes in watersheds with hydrological data.

A 41-year discharge data series (1981–2022) was used for simulating the Chari-Logone basin, with a 12-year calibration period (2010–2022) and a 29-year validation period (1981–2009). In both cases, a model stabilization period (spin-up) of approximately 2 years (2010–2011 and 1981–1982) is considered to reduce uncertainties related to the initial conditions of the model parameters^{44,45}.

To assess the sensitivity of the model's parametrization, a qualitative analysis was conducted by measuring the model performance through a comparison of the modelled and observed data. To achieve this, four performance criteria were utilized as follows:

1. The Nash–Sutcliffe efficiency coefficient (NSE):

$$NSE = 1 - \frac{\sum_{i=1}^N (o_i - s_i)^2}{\sum_{i=1}^N (o_i - \bar{o})^2}$$

where N is the length of the simulation and observation period, o_i and s_i are the observed and simulated data at time i , respectively, and \bar{o} represents the mean of the observed values. NSE values greater than 0.75 were classified as good, while values between 0.4 and 0.75 were considered acceptable^{45,46}.

2. The Kling-Gupta efficiency coefficient (KGE):

$$KGE = 1 - \sqrt{(r - 1)^2 + \left(\frac{\sigma_s}{\sigma_o} - 1\right)^2 + \left(\frac{\mu_s}{\mu_o} - 1\right)^2}$$

where r is the Pearson correlation coefficient, σ_s and σ_o are the standard deviations of the simulated and observed values, respectively, and μ_s and μ_o are the means of the simulated and observed values.

3. The percentage bias (PBIAS):

$$PBIAS = 100 \times \frac{\sum_{i=1}^N o_i - s_i}{\sum_{i=1}^N o_i}$$

where N is the length of the simulation and observation period and o_i and s_i are the observed and simulated data, respectively, at time i . Negative and positive PBIAS values indicate underestimation and overestimation of the simulated discharge compared to the observed discharge. Values of $|\text{PBIAS}| < 20\%$ are considered good⁴⁶.

4. The root mean square error (RMSE):

$$RMSE = \sqrt{\frac{1}{N} \sum_{i=1}^N (o_i - s_i)^2}$$

where N is the length of the simulation and observation period.

CMIP6 models and scenarios

Shared socioeconomic pathway (SSP) scenarios are narratives that describe possible developments in future society and were established by the IPCC as a common framework for climate projections. These models are based on socioeconomic assumptions, such as population growth, education, urbanization and GDP. The SSP scenarios range from SSP1 to SSP5 from more optimistic to less optimistic in terms of radiative forcing outcomes. Each SSP scenario can be assigned radiative forcing (in W/m^2) for the year 2100, which is produced by the increase in greenhouse gases according to the different SSP assumptions.

Two scenarios were chosen for this study: SSP245 and SSP370. SSP245 corresponds to the current consensus trajectory. SSP370 corresponds to a pessimistic scenario. From a risk management point of view, this scenario may be of interest for assessing the impact of more abrupt climate change on flooding in N'Djamena. The various estimated average degrees of global warming for the scenarios relative to the period of 1850–1900 are between 2.1 °C and 3.5 °C by 2100 for SSP245 (corresponding to the 4.5 W/m^2 forcing level in 2100). For SSP370, the temperature is between 2.8 °C and 4.5 °C by 2100 (corresponding to 7.0 W/m^2 radiative forcing).

Estimations of future flows on the Chari-Logone platform are based on rainfall-flow modelling (“The MGB model”) forced by rainfall from the CMIP6 (Couple Model Intercomparison Project Phase 6) future climate scenarios. To select the most suitable CMIP6 models for the study region, we relied on several studies that assessed the quality of the models for representing precipitation in West Africa^{47–50}. We selected the following models: IPSL.CM6-LR, NESM3, CMCC.CM2-SR5, ACCESS-CM2 and MIROC-ES2L (see Supplementary Table S3 for details). These models have a low rainfall bias compared with the observations at the sites studied in the references.

Rainfall correction Climate models are substantial simplifications of real-world climate conditions. Although they are based on physical principles, they involve numerical approximations, particularly semiempirical parametrizations of subgrid processes. Convection parametrization is especially significant, as convection-driven rainfall is the main source of precipitation in the region. These simplifications can lead to considerable errors, often preventing the direct incorporation of climate model results in impact studies. Despite the relatively low bias in the chosen models, it is necessary to correct this bias to carry out impact studies on hydrology⁵¹. Precipitation from CMIP6 models shows biases for annual accumulation and extreme events.

There are several bias correction methods, but the one that yields the best results is quantile mapping⁵². This method involves adjusting the quantiles of observed and model-simulated distributions⁵³. It has been recurrently applied in the literature for hydrological impact studies⁵⁴.

To correct for rainfall from the CMIP6 models, we proceeded as follows:

Step 1: Use of the CHIRPSv2 precipitation data as an observation reference (daily data series from 1981 to present at a 0.25° resolution).

Step 2: Calculate the spatial average of daily precipitation over the Chari-Logone basin for observed rainfall and the historical period of the CMIP6 models.

Step 3: Calculate the rainfall thresholds to match the number of wet days from the reference.

Step 4: Calculate the quantiles of observed rainfall distribution by month. Different corrections are applied depending on the period of the season to correct bias related to season dynamics.

Step 5: Apply the wet-day threshold and quantile-quantile correction coefficients to the CMIP6 model to match the quantiles in the historical period and projections.

Supplementary Figure S8 shows the effect of the correction for the period of 1981–2022. We observe an intraseasonal dependency on the model biases. For example, CMCC and MIROC show large rainfall positive biases at the beginning of the season (February–June) and negative biases during the core rainfall season (July–September).

Flow rate correction Based on flow (height) observations from hydrometric stations and MGB model simulations, the following flow records are available downstream and upstream of the confluence of the Chari and Logone Rivers at N'Djamena:

Q_0 : observed flows (1933–2022, depending on the station)

Q_R : flows reconstructed by the MGB model from CHIRPSv2 rainfall (period: 1981–2022, calibration over the period of 2010–2022)

Q_H : historical flows simulated from debiased CMIP6 rainfall (1950–2014)

Q_F : simulated prospective flows from debiased CMIP6 rainfall (2015–2100).

The aim of this section is to describe the methodology used to estimate the evolution of peak flows in the Chari and Logone Rivers in past and future climates. The methodology is based on the evolutionary estimation of the distributions of annual flow maxima (peak flow) over 25-year sliding windows. For this purpose, we used the generalized extreme value distribution (GEV) from extreme value theory, which is a generalization of the Gumbel law described in "The percentage bias (PBIAS):" and is commonly used to describe the distribution of extremes. The GEV law was fitted to the above-described annual peak flows $Q_{Q_X}^{max}$ for 25 years of sliding windows, y . The probability density of the GEV law, $F(x)$, can be written as

$$F(s, \xi) = \exp\left(-(1 + \xi s)^{-1/\xi}\right)$$

With $\xi \neq 0$ $s = (x - \mu) / \sigma$

$[\mu, \sigma, \xi]$ are the three parameters of the law.

$\mu \in R$: location parameter (related to the mean and median).

$\sigma > 0$: scale parameter (related to the variance).

$\xi \in R$: shape parameter.

If $\xi = 0$, we have the special case of the Gumbel distribution of extremes.

The parameters $[\mu, \sigma, \xi]$ were estimated using maximum-likelihood fitting with the annual peak flow for 25-year windows.

Flows are linked to seasonal accumulations in the basin. These accumulations varied over the course of the twentieth century: during the 1970s and 1980s, there was a decrease in accumulation, which increased again in the following decades. To consider the multidecadal variations in past and future developments due to climate change, we chose to fit a GEV law over a 25-year sliding window. Therefore, over a period $[t_0 - 12; t_0 + 12]$ for each year t_0 , we can define the flow Q with a return period T as follows:

$$F(Q_T) = 1 - 1/T$$

Once we have adjusted GEV's parameters, we can write the flows' return periods as follows:

$$Q_T = \mu + \sigma/\xi \left[(-\log(1 - 1/T))^{-\xi} - 1\right]$$

The fitting of GEV laws over a 25-year period does not allow us to robustly trace return periods greater than 25 years due to the uncertainty surrounding the estimation of parameters on such a small sample. Additionally, reconstructed annual maximum flows Q_R^{Max} are biased with respect to observed flows Q_0^{Max} . This bias can be attributed to the bias of the MGB model under the assumption that the CHIRPSv2 rainfall data have little bias (adjusted by rain gauges). This peak flow bias is visible in Fig. 5 (main text) in the gap between the pink solid line (observed return flows) and the brown calibration and validation period (Q_R^{Max}).

The historical peak annual flows derived from simulations Q_H^{Max} are biased with respect to the reconstructed flows Q_R^{Max} . These biases can be attributed to the CMIP6 models. Even with rainfall debiasing, the annual dynamics and spatial distributions of rainfall may be erroneous in the models, producing biases in the flood peak. To avoid various biases, we consider only the relative evolution of the datasets.

To compare prospective flows at different return periods derived from the MGB model (Q_F) with observed flows Q_0 , we corrected the parameter μ_F extracted from the GEV adjustments of the prospective flow series. By doing so, we correct the biases derived from the model and projections empirically. We adjusted the parameter μ_F of the prospective flow from each CMIP6 model for the period of 2005–2015:

$$\mu_F^c = \mu_F$$

Data availability

The datasets used and/or analysed during the current study available from the corresponding author on request.

Received: 26 February 2024; Accepted: 8 October 2024

Published online: 20 October 2024

References

1. Shanahan, T. M. et al. Atlantic forcing of persistent drought in West Africa. *Science* **324**, 377–380 (2009).
2. Lebel, T. & Abdou, A. Recent trends in the Central and Western Sahel rainfall regime (1990–2007). *J. Hydrol.* **375**, 52–64 (2009).
3. Maharana, P., Younous Abdel-Lathif, A. & Charan Pattanayak, K. Observed climate variability over Chad using multiple observational and reanalysis datasets. *Glob. Planet. Change.* **162**, 252–265 (2018).
4. Giorgi, F. Variability and trends of sub-continental scale surface climate in the twentieth century. Part I: observations. *Clim. Dyn.* **18**, 675–691 (2002).
5. Dai, A. et al. The recent Sahel drought is real. *Int. J. Climatol.* **24**, 1323–1331 (2004).
6. Nicholson, S. On the question of the "recovery" of the rains in the West African Sahel. *J. Arid Environ.* **63**, 615–641 (2005).
7. Gbetkom, P. G. et al. Lake Chad vegetation cover and surface water variations in response to rainfall fluctuations under recent climate conditions (2000–2020). *Sci. Total Environ.* **857**, 159302 (2022).
8. Panthou, G., Vischel, T. & Lebel, T. Recent trends in the regime of extreme rainfall in the Central Sahel. *Int. J. Climatol.* **34**, 3998–4006 (2014).
9. Taylor, C. M. et al. Frequency of extreme Sahelian storms tripled since 1982 in satellite observations. *Nature* **544**, 475–480 (2017).
10. Sighomnou, D. et al. La crue de 2012 à Niamey : un paroxysme du paradoxe du Sahel ?. *Sècheresse* **24**, 3–13 (2013).

11. Epule, T. E., Ford, J. D. & Lwasa, S. Climate change stressors in the Sahel. *GeoJournal* **83**, 1411–1424 (2018).
12. IPCC Climate Change 2021: The Physical Science Basis. *Contribution of Working Group I to the Sixth Assessment Report of the Intergovernmental Panel on Climate Change* (eds. Masson-Delmotte, V., et al.) (Cambridge University Press, 2021).
13. UNHCR <https://www.unhcr.org/news/briefing-notes/millions-face-harm-flooding-across-west-and-central-africa-unhcr-warns> (2022).
14. Centre Régional AGRHYMET http://agrhymet.ciilss.int/wp-content/uploads/2022/06/Bulletin_PRESASS22 (2022).
15. Africa News <https://www.africanews.com/2022/09/19/nearly-160-dead-and-225-000-affected-in-nigers-rains/> (2022).
16. Ruth <https://www.nytimes.com/2022/10/17/world/africa/nigeria-floods.html> (2022).
17. Akbarzai, S., Smith, K. & McCluskey, M. <https://edition.cnn.com/2022/10/17/africa/nigeria-floods-deaths-intl-hnk/index.html> (2022).
18. Balogun, R. A., Adefisan, E. A., Adeyewa, Z. D. & Okogbue, E. C. Thermodynamic environment during the 2009 Burkina Faso and 2012 Nigeria Flood Disasters: Case study. In *African Handbook of Climate Change Adaptation* (eds Oguge, N. et al.) 1705–1720 (Springer, 2021).
19. The conversation <https://theconversation.com/nigeria-floods-expert-insights-into-why-theyre-so-devastating-and-what-to-do-about-them-192409> (2022).
20. Telesur English <https://www.telesurenglish.net/news/612-People-Killed-in-Floods-Across-Nigeria-20221026-0002.html> (2022).
21. OCHA, Chad Rapport de situation <https://response.reliefweb.int/chad> (2022).
22. France 24 <https://www.france24.com/fr/afrique/20221020-au-tchad-le-pr%C3%A9sident-d%C3%A9cr%C3%A8te-un-%C3%A9tat-d-urgence-face-aux-inondations> (2022).
23. Pham, B. et al. The Lake Chad hydrology under current climate change. *Sci. Rep.* **10**, 5498 (2020).
24. Mahamat Nour, A. et al. Dynamic and geochemical behavior of the dissolved load of the Chari -Logone river in the Lake Chad basin. *Aquat. Geochem.* <https://doi.org/10.1007/s10498-019-09363-w> (2019).
25. Bader, J. C., Lemoalle, J. & Leblanc, M. Modèle hydrologique du lac Tchad. *Hydrol. Sci. J.* **56**, 411–425 (2011).
26. Olivry, J. C., Chouret, A., Vuillaume, G., Lemoalle, J. & Bricquet, J. P. Hydrologie du Lac Tchad. Monographies hydrologiques, édition ORSTOM, Paris (1996).
27. Bouchez, C. et al. Hydrological, chemical and isotopic budgets of Lake Chad: a quantitative assessment of evaporation, transpiration and infiltration fluxes. *Hydrol. Earth Syst. Sci.* **20**, 1599–1619 (2016).
28. Nicholson, S. E. On the factors modulating the intensity of the tropical rainbelt over West Africa. *Int. J. Climatol.* **29**, 673–689 (2009).
29. Cornforth, R. et al. Synoptic systems. In *Meteorology of Tropical West Africa* 40–89 (Wiley, 2017).
30. Giorgi, F. et al. Higher hydroclimatic intensity with global warming. *J. Clim.* **24**, 5309–5324.
31. Panthou, G. et al. Rainfall intensification in tropical semi-arid regions: the Sahelian case. *Environ. Res. Lett.* **13**, 064013 (2018).
32. Zachariah, M. et al. Climate change exacerbated heavy rainfall leading to large scale flooding in highly vulnerable communities in West Africa. World Weather Attribution <https://www.worldweatherattribution.org/climate-change-exacerbated-heavy-rainfall-leading-to-large-scale-flooding-in-highly-vulnerable-communities-in-west-africa/> (2022).
33. Dosio, A. et al. What can we know about future precipitation in Africa? Robustness, significance and added value of projections from a large ensemble of regional climate models. *Clim. Dyn.* **53**, 5833–5858 (2019).
34. RGPH2, Recensement Général de la population et de l'habitat, Institut National de la statistique, des études économiques et démographiques (INSEED) (2009).
35. Clement, V. et al. Groundswell Part 2: Acting on Internal Climate Migration. World Bank, Washington, DC. <http://hdl.handle.net/10986/36248> (2021).
36. Vermote, E. MOD09A1 MODIS Surface Reflectance 8-Day L3 Global 500m SIN Grid V006. NASA EOSDIS Land Processes DAAC (2015).
37. Berge-Nguyen, M. & Cretaux, J.-F. Inundations in the inner Niger delta: Monitoring and analysis using MODIS and global precipitation datasets. *Remote Sens.* **7**, 2127–2151 (2015).
38. Sakamoto, T. et al. Detecting temporal changes in the extent of annual flooding within the Cambodia and the Vietnamese Mekong Delta from MODIS time-series imagery. *Remote Sens. Environ.* **109**, 295–313 (2007).
39. Crétaux, J.-F. et al. Lake volume monitoring from space. *Surveys Geophys.* **37**, 269–305 (2016).
40. Collischonn, W., Allasia, D., Da Silva, B. C. & Tucci, C. E. The MGB-IPH model for large-scale rainfall—runoff modelling. *Hydrol. Sci. J.* **52**, 878–895 (2007).
41. Getirana, A. C. et al. Hydrological monitoring of poorly gauged basins based on rainfall—runoff modeling and spatial altimetry. *J. Hydrol.* **379**, 205–219 (2009).
42. Paiva, R. C., Collischonn, W. & Tucci, C. E. Large scale hydrologic and hydrodynamic modeling using limited data and a GIS based approach. *J. Hydrol.* **406**, 170–181 (2011).
43. Beven, K. & Freer, J. Equifinality, data assimilation, and uncertainty estimation in mechanistic modelling of complex environmental systems using the GLUE methodology. *J. Hydrol.* **249**, 11–29 (2001).
44. Collischonn, W. Simulação hidrológica de grandes bacias. PhD Thesis—Instituto de Pesquisas Hidráulicas, Universidade Federal do Rio Grande do Sul (IPH-UFRGS), Porto Alegre, Brazil, 270 (2001).
45. Tucci, C. E. M., Clarke, R. T., Collischonn, W., Dias, P. L. S. & Sampaio, G. Long term flow forecast based on climate and hydrological modeling: Uruguay River basin. *Water Resour. Res.* **39**, 1181. <https://doi.org/10.1029/2003WR002074> (2003).
46. Van Liew, M. W., Arnold, J. G. & Garbrecht, J. D. Hydrologic simulation on agricultural watersheds: Choosing between two models. *Trans. ASAE* **46**, 1539–1551 (2003).
47. Pereira, D. D. R. et al. Hydrological simulation using SWAT model in headwater basin in Southeast Brazil. *Engenharia Agrícola* **34**, 789–799 (2014).
48. Shiru, M. S. & Chung, E. S. Performance evaluation of CMIP6 global climate models for selecting models for climate projection over Nigeria. *Theoret. Appl. Climatol.* **146**, 599–615 (2021).
49. Agyekum, J., Annor, T., Quansah, E., Lamptey, B. & Okafor, G. Extreme precipitation indices over the Volta Basin: CMIP6 model evaluation. *Sci. Afr.* **16**, e01181 (2022).
50. IPCC, 2015: Workshop Report of the Intergovernmental Panel on Climate Change Workshop on Regional Climate Projections and their Use in Impacts and Risk Analysis Studies (eds. Stocker, T.F. et al.) 171 (IPCC Working Group I Technical Support Unit, University of Bern, 2015).
51. Rameshwaran, P., Bell, V. A., Davies, H. N. & Kay, A. L. How might climate change affect river flows across West Africa?. *Clim. Change* **169**, 21 (2021).
52. Teutschbein, C. & Seibert, J. Bias correction of regional climate model simulations for hydrological climate-change impact studies: Review and evaluation of different methods. *J. Hydrol.* **456**, 12–29 (2012).
53. Worku, G., Teferi, E., Bantider, A. & Dile, Y. T. Statistical bias correction of regional climate model simulations for climate change projection in the Jemma sub-basin, upper Blue Nile Basin of Ethiopia. *Theoret. Appl. Climatol.* **139**, 1569–1588 (2020).
54. Azmat, M., Qamar, M. U., Huggel, C. & Hussain, E. Future climate and cryosphere impacts on the hydrology of a scarcely gauged catchment on the Jhelum river basin, Northern Pakistan. *Sci. Total Environ.* **639**, 961–976 (2018).

Acknowledgements

This study was funded by the French National Research Institute for Sustainable Development (IRD, France) and the University of N'Djamena (Chad). The modelling experiment was part of the project funded by the World Bank and coordinated by EGIS (Montpellier, France). The authors are grateful to the Lake Chad Basin Commission Basin (LCBC), the Chadian Ministry of Urban and Rural Hydraulic, and the Chadian National Meteorological Agency for providing observations, data and facilities in the field. The authors are grateful to NASA and the ESA for providing satellite observations and to the Centre for Topographic Studies of the Oceans and Hydrosphere (CTOH, www.legos.obs-mip.fr/observations/ctoh) at LEGOS (Toulouse, France) for providing altimetry data in a standard and useful form from the Hydroweb site. The authors are also grateful to the French Embassy in Chad and its support from the French Ministry of Europe and Foreign Affairs.

Author contributions

F.S. designed the study. F.S., A.M.N., T.N., D.G. and M.M.A. provided the hydrological data. B.P.D. and J.-F.C. provided the satellite imagery and altimetry data from Lake Chad. A.M.N. estimated the return flood period. M.A., L.G. and A.P. designed the modelling experiment and climatic projections. C.L. and R.R. contributed to the interpretation of the hydrological data and the modelling experiments. F.S. prepared the original manuscript, and all the authors contributed to the discussion of the results and commented on the manuscript.

Competing interests

The authors declare no competing interests.

Additional information

Supplementary Information The online version contains supplementary material available at <https://doi.org/10.1038/s41598-024-75707-4>.

Correspondence and requests for materials should be addressed to F.S.

Reprints and permissions information is available at www.nature.com/reprints.

Publisher's note Springer Nature remains neutral with regard to jurisdictional claims in published maps and institutional affiliations.

Open Access This article is licensed under a Creative Commons Attribution-NonCommercial-NoDerivatives 4.0 International License, which permits any non-commercial use, sharing, distribution and reproduction in any medium or format, as long as you give appropriate credit to the original author(s) and the source, provide a link to the Creative Commons licence, and indicate if you modified the licensed material. You do not have permission under this licence to share adapted material derived from this article or parts of it. The images or other third party material in this article are included in the article's Creative Commons licence, unless indicated otherwise in a credit line to the material. If material is not included in the article's Creative Commons licence and your intended use is not permitted by statutory regulation or exceeds the permitted use, you will need to obtain permission directly from the copyright holder. To view a copy of this licence, visit <http://creativecommons.org/licenses/by-nc-nd/4.0/>.

© The Author(s) 2024